JOURNAL OF PROPULSION AND POWER
Vol. 11, No. 6, November–December 1995

Supersonic Combustion Ramjet Missile

Frederick S. Billig*
Johns Hopkins University, Applied Physics Laboratory, Laurel, Maryland 20723

During the period of 1962–1978, the Applied Physics Laboratory of Johns Hopkins University developed the technology for a family of missiles named SCRAM for use as fleet defense weapons. SCRAM is the acronym for supersonic combustion ramjet missile. The development work began with the conceptual design of two missile configurations and calculations of the expected performance for a variety of missions to provide defense for the surface fleet. A novel class of multimodule fixed-geometry hypersonic inlets was designed and wind-tunnel models were built and tested at Mach numbers of 4–10 at angles of attack up to 15 deg. Injector and combustor development was carried out in direct connect test apparatus. Considerable effort was directed to the development and testing of a wide variety of storable, reactive liquid fuels including boranes and aluminum alkyls. Many new testing techniques and diagnostic instruments were developed that are still key elements of scramjet test operations. The program culminated with the testing of the entire engine in free jets at Mach numbers of 5–7.3 and the design of a family of revised vehicle configurations that could exploit the full capability of the performance observed in the ground test program. This article presents the highlights of the technology program and references recently released documents.

Nomenclature

A	=	cross-sectional area
A_R	=	reference area
C_{DADD}	=	additive drag, D_{ADD}/q_0A_R
C_T	=	thrust coefficient, T/q_0A
L_c, L_d, L_i, L_n	=	lengths defined in Fig. 14
M	=	Mach number
M_a, M_{ci}	=	Mach number entering combustor
P_{ci}	=	static pressure at combustor entrance
P_{ta}	=	air total pressure
P_w	=	wall pressure
q	=	dynamic pressure
T_{ci}	=	static temperature at combustor inlet
T_f	=	fuel temperature
T_{ta}, T_{to}	=	air total temperature
η_c	=	combustion efficiency

Introduction

FOLLOWING the pioneering work at the NASA Lewis Research Center in the mid-1950s,[1,2] the Applied Physics Laboratory of Johns Hopkins University (JHU/APL) initiated an investigation of combustion in external supersonic streams. Highly reactive fuels were injected adjacent to wedge airfoils and vigorous burning was observed.[3,4] Considerable lift and some thrust were produced in tests at Mach 5. However, both the experimental results and complementary analytical studies showed that whereas external burning was a viable means for generating lift and canceling drag, the efficiency was unacceptably low if net thrust was required. Nonetheless, the encouraging result of the demonstration of stable combustion in supersonic flow prompted the investigators to examine the feasibility of an internally burning supersonic combustion ramjet (a scramjet). The analytical studies that followed[5,6] and those conducted elsewhere[7] concluded that a scramjet could produce net thrust and would be more efficient than a conventional subsonic burning ramjet at Mach numbers above 6–8.

Based on these studies and some very successful early tests of ducted supersonic combustors, preliminary conceptual designs of scramjet-powered missiles were undertaken in 1961. In the initially proposed configuration (which was disclosed), held under an order of secrecy and ultimately patented, a "conventional" asymmetric external–internal contraction inlet, was designated.[9] However, the weight and complexity of the variable geometry system required to assure inlet starting suggested that an alternative fixed-geometry inlet would be preferable for expendable lighter-weight missiles. The advent of a new class of inlets cut along streamline surfaces of internally contracting flowfields provided the catalyst for a pair of viable missile designs that were named SCRAM (supersonic combustion ramjet missile).[10,11] These inlets are self-starting and thereby eliminate the need for variable geometry.

Vehicle Designs and Performance

The two original configurations of the SCRAM weapon system are shown in Fig. 1. The primary mission of both

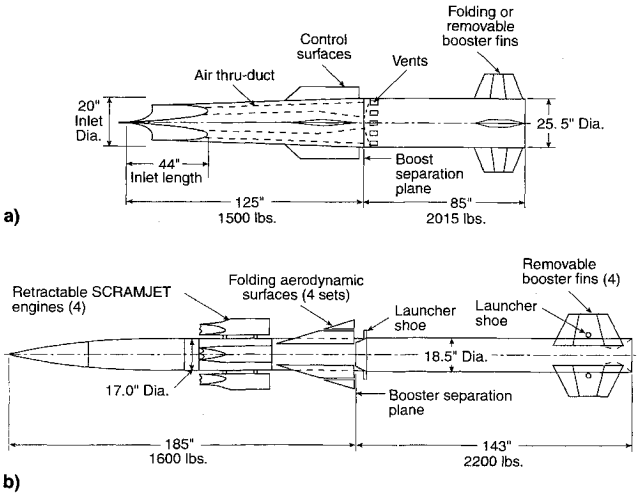

Fig. 1 Principal candidate SCRAM configurations: a) SCRAM-MOD 1 weapon and b) SCRAM-MOD 2 weapon (compatible with MK-10 GMLS).

Presented as Paper 93-2329 at the AIAA/SAE/ASME/ASEE 29th Joint Propulsion Conference, Monterey, CA, June 28–30, 1993; received Feb. 3, 1994; revision received Feb. 8, 1995; accepted for publication Feb. 10, 1995.

*Chief Scientist and Associate Aeronautics Department Head. Fellow AIAA.

weapon systems was defense of the surface fleet from airborne threats. MOD 1 (Fig. 1a) was sized to fit into the Talos MK12 launcher system and MOD 2 is compatible with the Terrier MK10 launcher. Both configurations are two stages with separable rocket boosters that accelerate the second-stage scramjets to takeover speeds of Mach 3.5–4. In MOD 1, the engine and missile are one, i.e., the other missile components are integrated within and around a four-module, nose-inlet engine, and the engine exhaust from the four modules essentially fills the missile base region. This configuration has good acceleration capabilities due to its large ratio of inlet-capture area to missile weight, but its low-length/diameter ratio presents aerodynamic characteristics that indicate a need for large tails for control. In MOD 2 all other missile components are packaged in an ogive-cylinder body and four podded engines are used. In stowage, the engines are semisubmerged in a section of the body. They are automatically swung out to the flight position indicated in the sketch while the missile is on the launcher. The relative advantages and disadvantages of the two configurations are discussed in Ref. 12.

Figures 2 and 3 show inboard profiles and frontal views of the two configurations. An irregular fuel tank shape would be needed in MOD 1, whereas a simpler structurally efficient shape would be used in MOD 2 to contain the 350 lb of usable fuel. Different approaches would also be taken in the design of the respective guidance systems. MOD 1 could readily accommodate interferometer lenses on the inlet tips. MOD 2 would ideally be suited for a dish and radome.

The performance envelope of SCRAM is shown in Fig. 4. It is based on acceleration to Mach 6.5 at sea level and Mach 8.5 at high altitude. Whereas these speeds would be attainable with the accelerative capability of the engines, materials development has not progressed to the level envisioned by the engineering community in the 1960s. These speeds were chosen to correspond to a 3800°F temperature on external stagnation points on the missile. This was the highest temperature believed possible with coated materials. Contemporary studies suggest limits of about Mach 5.5–6 at sea level and Mach 6.5–7 at altitude for passively cooled structures. These lower limits would move the time lines to the left and the straight line engine out and coasting to Mach 4 lines to the right. Nonetheless, the general features of a scramjet-powered vehicle are depicted. Either SCRAM configuration could carry a 125–145-lb warhead to the radar horizon in sea-level flight at average Mach numbers greater than 6. Either could attain ranges exceeding 400 nm at cruise altitudes near 100,000 ft at average Mach numbers greater than 8. With a 100-*g* booster SCRAM, MOD 1 could reach 118,000 ft in 15 s; MOD 2 would reach 93,000 ft in the same time. To intercept at low-altitude targets at long range, the missile would fly at the optimum cruise altitude and then dive. The greatest performance advantage of SCRAM, compared to an equally advanced rocket missile of the same size, would be for missions requiring flight at low altitude or along low-angle, line-of-sight (minimum time-to-target) flight paths. For on-the-deck flight at Mach 6.5, SCRAM would have approximately twice the range of a rocket and along low-angle paths it would have about three times the powered range of a rocket. It would also outperform a subsonic combustion ramjet at hypersonic speeds because of its higher fuel-specific impulse, and it would have internal pressures that are lower by a factor of 4–5; hence, structural design requirements would be greatly relieved.

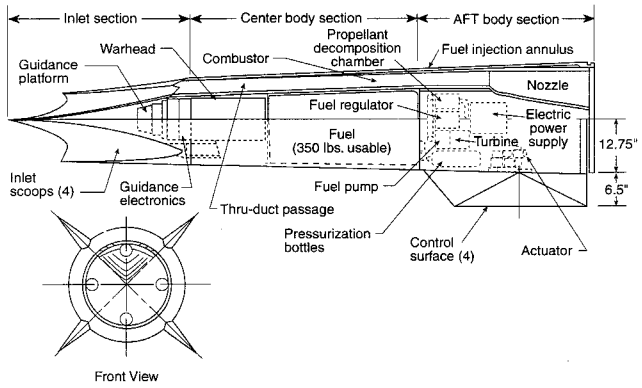

Fig. 2 Inboard profile SCRAM MOD 1 missile.

The performance estimates shown in Fig. 4 were based on the use of an alkylated liquid borane fuel, HiCal-3D ($C_{3.2}H_{20.3}B_{10}$) having a molecular weight of 166.54, a density of 51.2 lb/ft^3, and lower heating values of 25,960 Btu/lb and 1,329,000 Btu/ft^3. Most of the experimental program was carried out with this fuel, but others were examined to compare ignition and combustion characteristics.[12,13]

During the 1970s, many other configurations of SCRAM were examined with the objectives of simplifying the structural design and increasing the vehicle performance. Lower maximum speeds were examined as the reality of a less-than-expected materials capability became apparent.[11,14,15] Particular emphasis was given to designs that were compatible with the vertical box launchers that were being introduced into the newer naval vessels. Performance gains above those of all-rocket-powered systems were consistently predicted.

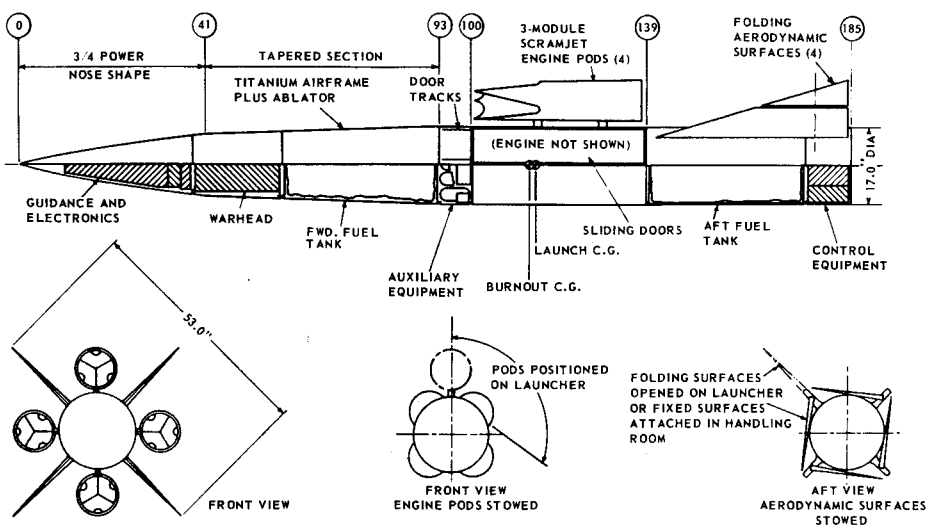

Fig. 3 External and inboard profiles SCRAM MOD 2 missile.

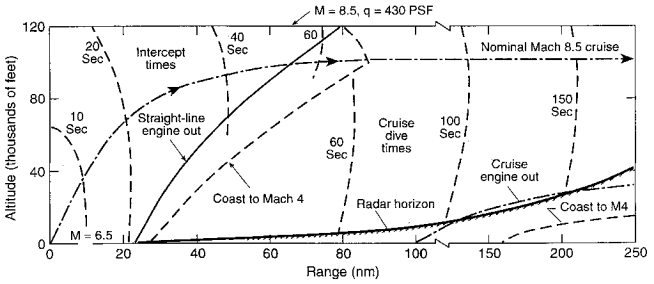

Fig. 4 SCRAM performance envelope.

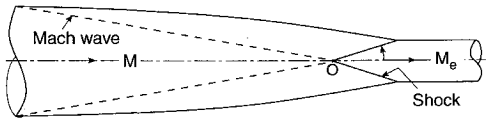

Fig. 5 Busemann inlet.

Experimental Test Program

The SCRAM development program, initiated in 1961, was comprised of four major elements: 1) design and wind-tunnel testings of modular inlets, 2) direct-connect tests of a large number of injector/combustor configurations, 3) design of a maximum thrust exhaust nozzle, and 4) freejet testing of the entire engine.

The design of the inlet for a hypersonic missile introduces some formidable challenges. To obtain high efficiency, the ratio of the cross-sectional area of the flow as it is compressed in the inlet must be relatively high at cruise conditions and relatively low at the end of boost. For a fixed-geometry device, this necessitates large supersonic spillover at the lower flight speeds. Outward turning flow must be followed by inward turning compression waves to yield near-axial flow in the combustor. This requires that at least a portion of the inlet compression be internal, which introduces starting problems at the end of boost. Exceedingly high heat transfer rates on leading edges suggest designs that employ sweep and thereby minimize stagnation points. All of these considerations led to the selection of the "crown"-type inlets for SCRAM.

The genera of the crown or Busemann inlet is an all-internally contracting flow. At the design Mach number the flow is compressed isentropically from a sharp leading edge along the inward turning walls as shown in Fig. 5. The isentropic compression waves coalesce on the axis of symmetry at point 0 in Fig. 5. Point 0 is also the apex of a conical shock that then turns all of the flow coaxially. At the design Mach number, the losses are minimal for this type of an internal compression inlet. At other Mach numbers, wave coalescence at a point is not realized and the terminal shock is not conical. Additional uncanceled compression and expansion waves are present and the corresponding efficiencies are lower than would be obtained in an "on-design" inlet. Nonetheless, the overall compression efficiency of these inlets is high relative to other types of compression fields. The fundamental problem is that the inlet will not start in steady flow. To circumvent this problem, the compression field can be cut into sectors along streamline surfaces and then reassembled into a viable shape suitable for a missile inlet. Figure 6 depicts this design strategy. The flowfield is thus segmented into discrete modules. In the upstream plane, the streamlines that are followed originate along the straight lines A-B and A-C and the circular arc B-O-C as shown in the front view. At the end of compression, the streamlines pass through X-Y-O-Z-X. The contoured inlet leading edges illustrated in the angular view are obtained by projecting lines AB, AC, and BOC onto the leading-edge Mach cone of the full inlet. Ahead of the intersection with the Mach cone, the surfaces are cut out; thus, the open-area B-O-C provides a zone for supersonic spillover

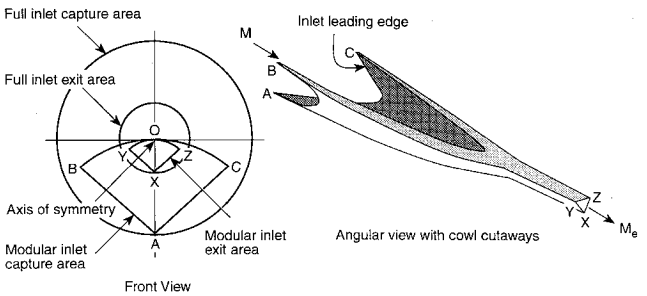

Fig. 6 Streamline tracing technique for design of modular Busemann inlet.

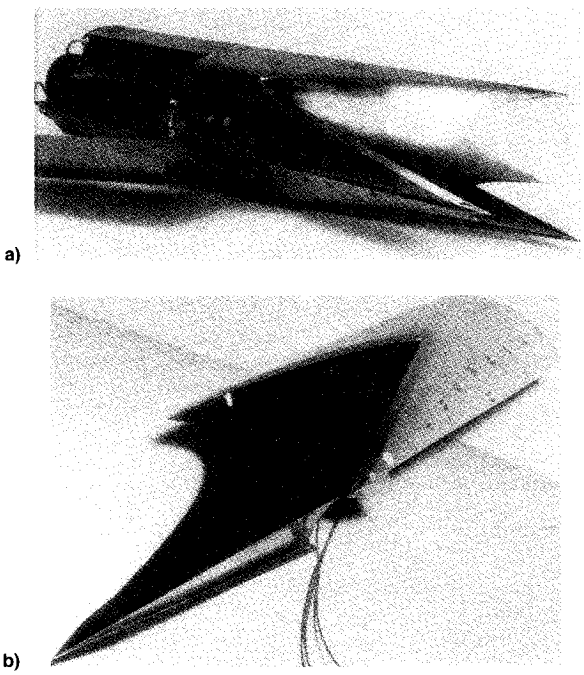

Fig. 7 SCRAM inlet test models: a) three-module inlet model and b) four-module inlet quadrant model.

when the inlet is operated below its design Mach number. The body of the inlet is then cut longitudinally along AB and AC and reassembled to form a four-module inlet that is cylindrical on the periphery. The angle B-A-C could be increased from 90 to 120 deg to form a three-module inlet or could be decreased to 72 deg for a five-module design, etc. For SCRAM, both three- and four-module inlet designs were tested. The three-module design, which was selected for the freejet engine tests, is ideally suited for a MOD 2 missile. The four-module inlet is optimal for MOD 1 and derived configurations.

Figure 7 shows photographs of the inlet test models and Table 1 summarizes the test results. These inlets had a design Mach number of 7.8 and were self-starting at Mach numbers below 4.

Whereas the cross-sectional shape of the flowfield at the exit of a segmented Busemann inlet is semielliptical, the direct-connect combustor tests were carried out in geometries with circular cross sections. It was hoped that an injector/combustor design that yielded high combustor efficiency in the direct-connect test would be only slightly modified and yield similar high efficiency in the freejet engine tests. This turned out to be the case.

Two experimental apparatus were used in the direct-connect test program, the principal difference being the air heater. A stainless-steel storage heater with a maximum operating temperature of 1850°F was used for tests simulating flight

Table 1 Summary of SCRAM inlet tests at zero angle of attack

Inlet type	Tested M	Tested Altitude, K ft	Air capture ratio	Kinetic energy efficiency
Three-module,	4.0	31	0.67	0.973
MOD 2	5.3	46	0.86	0.974
SCRAM	7.8	74	0.98	0.955
Four-module,	4.0	24	0.69	0.976
MOD 1	5.3	46	0.86	0.966
SCRAM	7.8	67	0.97	0.968
	10.0	98	0.98	0.953

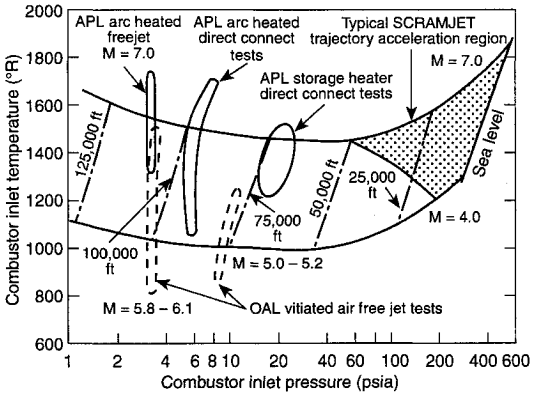

Fig. 8 Comparison of combustor inlet conditions for the SCRAM engine at altitudes between sea level and 125,000 ft for flight Mach numbers between 4–7 with various wind-tunnel test conditions.

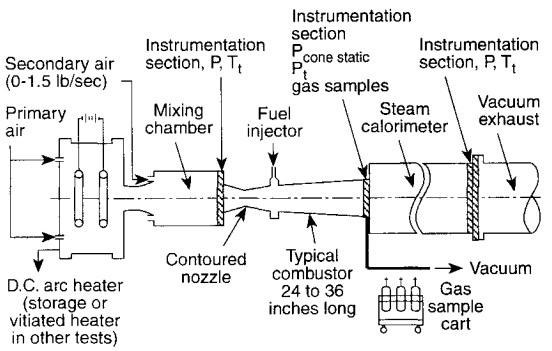

Fig. 9 Direct-connect test apparatus.

Mach numbers up to 5.[11–19] An electric arc heater provided the energy for higher Mach number tests. Figure 8 shows the regions of the flight envelope that were covered in the freejet and direct-connect test programs. Pressure and temperature are the coordinates of this figure to provide the reader an appreciation of the magnitudes of these key parameters that need to be simulated in ground tests of combustors.

The experimental apparatus used to simulate Mach 7, high-altitude SCRAM inlet conditions for the direct-connect combustor tests is depicted in Fig. 9. A metered airflow was heated in a dc electric-arc heater to approximately 4000–5500°R and passed through a mixing chamber where secondary air was added if necessary to lower the air total temperature T_{ta}. Air total pressure P_{ta} was measured directly in the mixing chamber and was typically 400–480 psia. A water-cooled, contoured Mach $3.2M_a$ nozzle with a 0.8675-in.^{2} throat was used between the mixing chamber and the combustor, yielding air weight flows of 3–3.2 lb. A two-throat method was used to deduce T_{ta} from the metered airflow, mixing chamber pressure measurements, and the continuity relationships for a supersonic nozzle.

Uncooled injector sections were followed by highly cooled combustor sections and a steam calorimeter. The longer water-jacketed combustors were fabricated from thin (0.062-in.) stainless-steel sheets and contained numerous wall thermocouples. Inside wall temperatures varied from 350–850°F in these sections, depending on test conditions and coolant rates. Shorter, thick-walled, water-cooled sections containing heat-flux calorimeters, pressure taps, and shear stress measuring apparatus were located between the longer sections in many tests. In-stream pitot and cone-static probes were located in the combustor exit plane to provide the necessary input into a momentum balance and stream-thrust efficiency determination. Immediately downstream of the combustor exit, water was sprayed into the stream for rapid quench of the products. The heat release and combustion efficiency were obtained by making a calorimetric balance on the exhaust gases using thermocouple measurements from a 16-point rake in the exit of the calorimeter together with all of the wall coolant rates. Water flow to the calorimeter was controlled to maintain rake temperatures of 700–1000°F in order to guarantee that liquid water would not be present and that the reactions would be quenched.

Literally hundreds of tests were made with a variety of injector geometrics, combustor configurations, and fuels.[11–19] Figure 10 is a typical static pressure distribution for tests with HiCal-3D showing the effect of combustor length on combustor efficiency. The injector geometry was 10 0.030-in.-diam holes equally spaced on the circumference of the 2.74 in. diameter. Immediately downstream of the injector section was stepped to a 3.28-in.-diam, 12-in.-long constant area section. This section was attached to one of two 1.4-deg half-angle conical sections. The shorter configuration was 13 in.

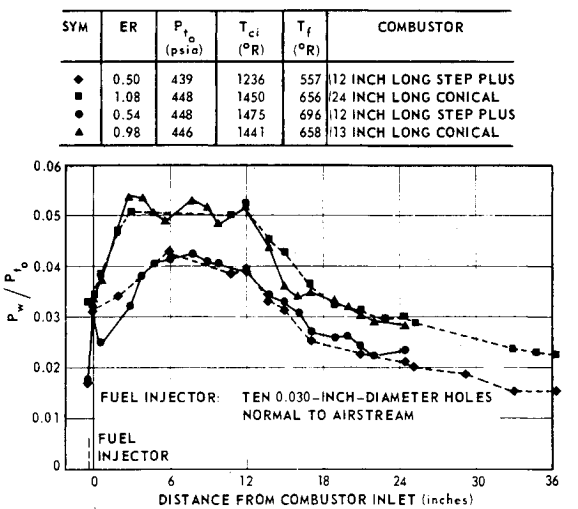

Fig. 10 Experimental combustor wall pressure distribution at M_{ci} = 3.2 with HiCal-3D fuel and step-cone combustor.

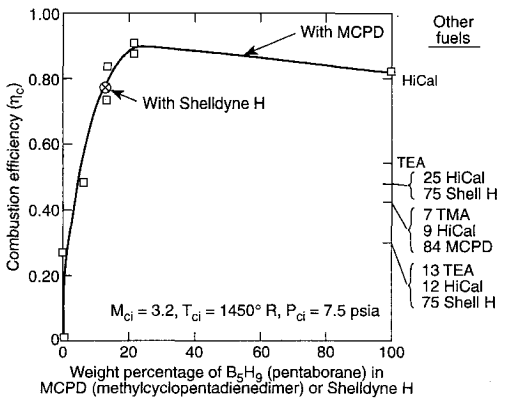

Fig. 11 Combustor efficiency in short-step combustor.

long, giving a total combustor length of 25 in.; the longer configuration had a 24-in.-long conical section and a total combustor length of 36 in. As expected, the additional length did not markedly alter the combustion process in the first 25 in. of length as indicated by the close proximity of the pressure plots. The anticipated result that occurred in the equivalence ratio (ER) ≈ 1 tests of an increase in combustion efficiency η_c was observed. At ER ≈ 0.5, no increase in η_c was noted in the longer configuration. This was attributed to a compensating effect due to lower air and fuel temperatures, 1236°R vs 1475°R, and 557°R and 696°R, respectively, in the longer combustor.

In another set of tests at approximately the same combustor inlet conditions, a number of different fuels and fuel blends were compared.[12] The combustor geometry was again a step-cylinder cone with the same step height, but with a cylinder length of 17.12 in. and a 1.4-deg cone frustum length of 14.34 in. Figure 11 shows η_c for blends of pentaborane B_5H_9 with either MCPD or Shelldyne H. MCPD is a dense hydrocarbon fuel (59.0 lb/ft^3, $C_{12}H_{16}$) with lower heating values of 17,905 Btu/lb and 1,056,000 Btu/ft^3. Shelldyne H is a denser hydrocarbon (67.5 lb/ft^3, $C_{14}H_{18}$) with lower heating values of 17,890 Btu/lb and 1,208,000 Btu/ft^3. The pure hydrocarbons either would not ignite or, if ignited, produced very little heat release. Adding (B_5H_9) increased η_c with a peak value at 20% by weight. Richer mixtures of B_5H_9 resulted in a slight decrease in η_c, but the decrease is within the accuracy of the η_c measurement. Results of other fuels and fuel blends are shown on the 100% B_5H_9 axis. With the exception of HiCal-3D, all other fuels tested had unacceptably low η_c values. It was these and similar results that showed the difficulty in burning fuels other than those containing boranes in the scramjet that led to the invention of the dual-combustor ramjet (DCR)[19] in 1977 at JHU/APL and the change in emphasis from SCRAM to the DCR in subsequent years. In the DCR engine, the inlet flow is bifurcated with about 25% directed to a subsonic combustor and the remainder to the main supersonic combustor. All of the fuel is added in the subsonic combustor and the resulting hot fuel-rich exhaust mixes and burns in the main supersonic combustor.

These data and the larger body of results from the cited references served to guide the design of the freejet engine. Moreover, the data served to guide the development of the modeling of supersonic combustion processes and establishing the versatility of the same.[20-24]

The design methodology for the nozzle of SCRAM was developed under contract.[25,26] A computer program using the method of characteristics with chemical reactions was developed to calculate numerous axis-symmetric nozzle expansions. Flow properties in the entrance plan were taken as uniform. The initial conditions were obtained from cycle calculations for the entire range of flight Mach numbers and engine-operating ER. Streamline surfaces were cut from the calculated flowfields in a similar method to that used in the inlet design. These surfaces were superposed and a compromised reference surface was adopted as shown in Fig. 12.[27] The other 15-deg half-angle conical shape was used in the initial tests of the SCRAM engine at Mach numbers of 5 and 5.8 because the contoured nozzle design technique had not yet been developed at the time. The improved performance materialized when the contoured nozzle was installed in SCRAM and tested at Mach 7.2 at JHU/APL. These results will be covered in the discussion of the freejet engine tests.

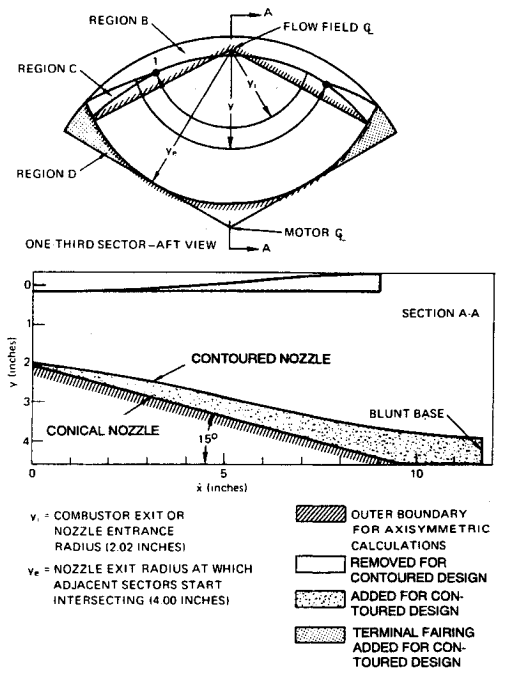

Fig. 12 SCRAM engine test model exhaust nozzle designs.

Freejet Engine Tests

Figure 13 is a photograph of the engine model with its outer skin removed, installed in the 15.2-in.-diam Mach 7 freejet nozzle at JHU/APL. The engine is comprised of a three-module (trifurcated) inlet, three semielliptic isolator duct modules, three combustor modules of semielliptical cross section, and a three-module contoured exit nozzle. It is an uncooled, thick-walled, heat-sink structure made for ground testing purposes. Except for the cowl-leading edges, the walls are 7/16-in. thick. The parts are made of Nickel 200 with the exception of molybdenum inlet tips and Haynes CD-752 columbium inserts located at the V-shaped junction of the inlet cowl (Fig. 7), which were used in tests at the Ordnance Aerophysics Laboratory in Dangerfield, Texas and at JHU/APL for air total temperatures $T_{ta} > 4000$°R. For $T_{ta} < 4000$°R, Nickel 200 inserts were used. The molybdenum and columbium components have discilicide coatings for oxidation protection at high temperature. The model is mounted on a sting support that rides on a thrust balance carriage. An independently mounted windscreen surrounds the sting and all of the instrumentation lines, fuel lines, and calorimeter cooling water lines, so that aerodynamic loads on these parts are isolated from the thrust measurements. With these provisions, thrust was resolved to ± 1 lb. A rake containing cone-static and pitot-pressure probes and gas-sampling probes was mounted in the engine nozzle-exit plane. Numerous static-pressure ports and thermocouples were located along the internal surfaces of the model together with a few water-cooled, 0.125-in.-diam, disk-type heat-flux calorimeters.

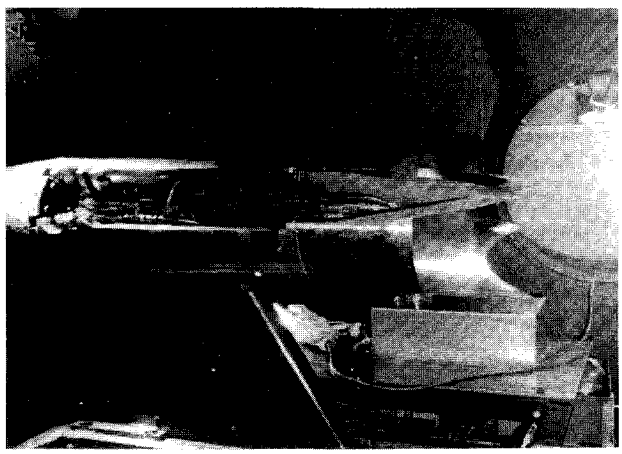

Fig. 13 SCRAM engine model in freejet with outer skin removed.

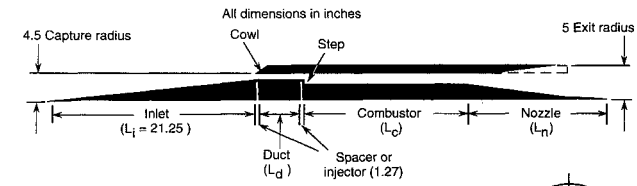

Model	L_d	L_c	L_n	Exit Nozzle	A_{ex}/A_{in}*
Taper	0.00	22.00	9.00	15° Conical	1.0000
Step	0.00	22.00	9.00	15° Conical	1.0000
Long-isolator-taper	13.50	22.00	9.00	15° Conical	1.0000
Long-isolator-step	13.50	22.00	9.00	15° Conical	1.0000
Short-isolator-step	3.50	18.25	15.00	Contoured	1.2346

* Model exit-to-inlet area ratio

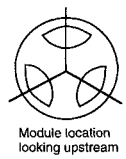

Dashed lines indicate conical nozzle
Taper–tapered combustor
Step–step combustor

Fig. 14 Schematic of APL freejet engines.

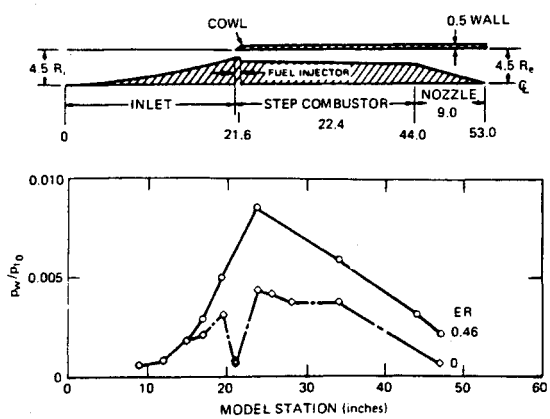

Fig. 15 Short engine configuration and longitudinal pressure distribution.

Figure 14 is a schematic illustration of a sectional view through one of the modules of the SCRAM engine. The table lists the important dimensions of the five configurations tested. In the taper and step configurations, the inlet was directly connected to the injector combustor. The long isolator was designed in accordance with the method described in Ref. 28 to accommodate the strongest shock train that occurred with high ER at $M_0 = 5.8$. The shorter isolator was designed to handle shock trains at $M_0 = 7$–7.3, where the strengths were considerably lower. The tests without an isolator were made to conclusively prove the necessity of the added duct length. The dashed line on the aft end of the cowl shows the initial outboard surface was tapered to eliminate base drag.

Figures 15 and 16 show typical longitudinal pressure traces for the step and long-isolator step configurations at Mach 5. The pressure trace for the no-fuel flow in the short configuration (Fig. 15) shows an increasing pressure on the external compression surface, followed by an abrupt decrease in pressure in the region of the step and then a recovery due to the subsequent cowl-reflected recompression waves. Farther downstream the pressure decreases, due primarily to the increasing cross-sectional area. With burning at ER = 0.46, the pressure rise of the precombustion shock is sufficiently large to separate the boundary layer on the intake's compression surface. This separated flow region, in turn, produced unwanted compression waves and additional air spillover and additive drag and increased pressure on the forward-facing surfaces on the inlet. With the long-isolator step configuration (Fig. 16), the character of the cold-flow trace is altered, reflecting the addition of the isolator. Instead of the pressure decrease at station 22, the pressure rises due to waves from the more highly compressed flow in the cowl region striking the inner surfaces in which the pressure taps are located. No pressure measurements were available in the region immediately downstream of the step or on the step base, and so

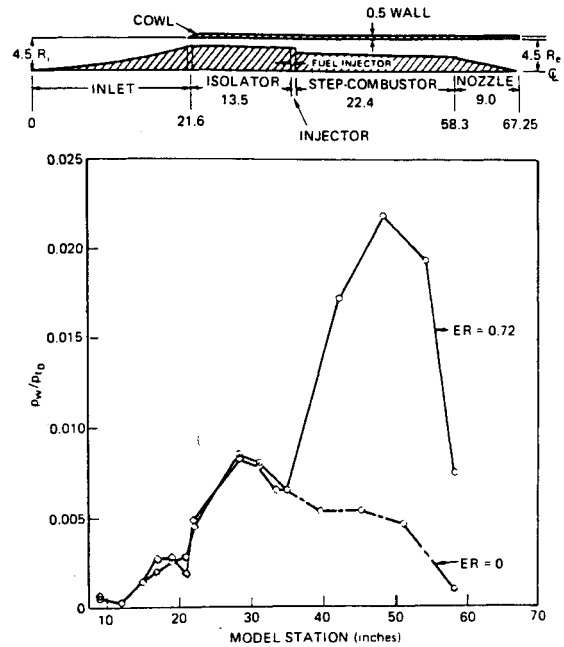

Fig. 16 Long engine configuration and longitudinal pressure distribution.

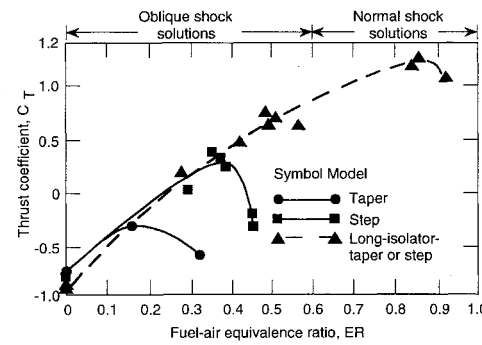

Fig. 17 Thrust coefficient of APL freejet engine at Mach 5.0.

whether or not a limited region of low pressure existed is not known. Pressures downstream of this point show the expected decreasing trend. With burning at ER = 0.72, the pressure rise at the combustor entrance is considerably stronger than at lower ER in the short configuration. However, this high pressure did not propagate forward onto the compression surfaces, thus establishing the adequacy of the isolation devices.

The strong impact of the interaction of combustion-induced disturbances on engine performance is shown in Fig. 17. Thrust coefficients for the first four configurations listed in the table on Fig. 13 are shown. In the short taper configuration, the maximum thrust coefficient $C_T = T/q_0A_R$, where $A_R = 78.54$ in.^{2}, occurred at ER = 0.15. Increasing the ER to 0.3 produced a region of reverse flow that was evidenced by a small flame zone on the external surfaces of the engine downstream of the cowl crotches. Further increase in ER caused a complete engine unstart and very large negative values of C_T (not shown). Changing the configuration to that having an abrupt step mitigated the adverse effect, moving the peak C_T to ER = 0.37. References 28 and 29 present compelling arguments that show that a step permits more heat release before reaching the same level of strength in the precombustion shock structure. With the long isolator installed in either the taper or step configuration, the engine could be operated satisfactorily over the entire ER range.

As the ER increases from 0 to about 0.6, the strength of the precombustion shock train increases from the equivalent

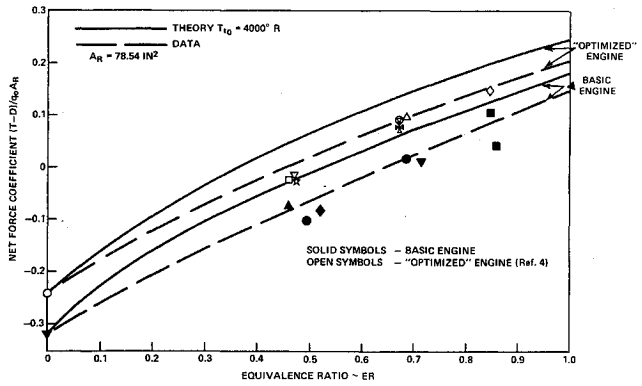

Fig. 18 Net force coefficients for hypersonic engine HiCal-3D fuel, M_0 = 6.91–7.02.

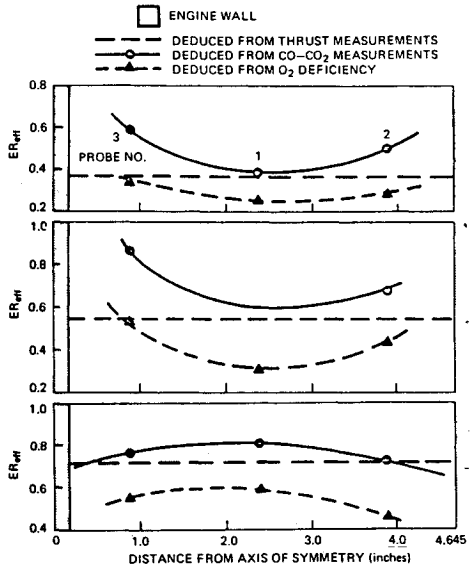

Fig. 19 Effective equivalence ratio (ER_{eff}) distribution along SCRAM engine module centerline.

of a weak oblique shock to a strong normal shock. Thus, the combustion process at low ER is supersonic and at high ER is subsonic. This transition, generally referred to as "dual mode" operation, was also observed in the tests at M_0 = 5.8 and 7–7.3.

Net force coefficients for tests with HiCal-3D fuel at Mach numbers of 6.91–7.02 are shown in Fig. 18. The theoretical curves are based on measured inlet efficiencies, calculated nozzle efficiencies, a specified combustion efficiency, calculated internal shear and heat losses, and external drags from aerodynamic wind-tunnel tests.[30] Additive drag coefficients $C_{DADD} = D_{DADD}/q_0A_R$ from the inlet tests are 0.0521 at T_t = 4000°R based on a reference area A_R = 78.54 in.^{2} External drags include a cowl-lip drag coefficient of 0.011, a friction drag of 0.035 for the short isolator-step geometry, and a base drag coefficient for the basic engine that varies from 0.002 at ER = 0 to −0.004 at ER_{eff} = 1. The correction for heat loss is quite significant, varying from an ER change of 0.05 at ER = 0 to 0.19 at ER = 1. The agreement between the measured and calculated net force coefficients at ER = 0 gives credence to the approach for estimating efficiencies and losses. The data points with combustion correspond to combustion efficiencies of 0.80–0.85. The expected increase in performance with the contoured exit nozzle in the "optimized" engine was observed and highlights the importance of nozzle design if maximum efficiency is to be realized in scramjet engines. The demonstration of thrust equal to drag at an ER = 0.5 in the optimized engine clearly establishes the viability of the scramjet as an effective accelerator to flight speeds greater than Mach 7.

Measurements made with the pitot-cone, static-gas sampling rake in the exit plane of the nozzle are typified by the data shown in Fig. 19. Two different methods for deducing the effective-equivalence ratio ER_{eff} from the gas samples were used. For the circles ER_{eff} is deduced from the ratio of the measured mass fractions of carbon to nitrogen, assuming there is no free carbon in the sample bottle. The triangle data points are based on the deficiency of oxygen as measured by the oxygen/nitrogen ratio, assuming that the NO hydrolyzes to HNO_3 in the presence of water in the sampling bottle. The NO fraction is taken as the value that is measured at ER = 0. The two sets of measurements are then compared with a mean value of ER_{eff} deduced from the thrust measurements. In general, the CO-CO_2 measurement is high and the O_2 measurement is low, but profiles are consistent in shape, thus giving a reasonable degree of confidence in the qualitative shapes of the fuel–air distributions. Considerably more details of the exit-plane measurements and techniques for data reduction are covered in the cited references.

Concluding Remarks

A very successful development program of scramjet-powered missiles for fleet defense was carried out during the period 1961–1978. Concepts for modular-inlet-combustor-nozzle configurations were conceived, design and analysis techniques were developed, and tests of the components verified the methods that were used. The components were successfully integrated into a viable engine design and tests of the engine in freejets at Mach 5–7.2 clearly demonstrated the feasibility of liquid-fueled scramjet engines. Some of the highlights of the test program and analysis thereof include the following:

1) A demonstration of the dual-mode engine concept; i.e., the operation in both the subsonic and supersonic combustion mode with smooth transition from one mode to the other.

2) The combustion efficiencies in the 80–90% range over the entire range 0 < ER ≤ 1.0.

3) A design procedure for combustor-inlet isolator that prevents undesirable interactions and minimizes shear and heat losses.

4) An accelerative capability that is equivalent to 11 g at Mach 5 sea level.

5) The development of instrumentation, measurement techniques, and cycle modeling that adequately describes the flow phenomena in a scramjet engine.

Since many of the cited references have only recently been downgraded and the publications in which they appear contain other classified papers, please contact the author directly at JHU/APL for copies.

References

[1]Dorsch, R. G., Serafini, J. S., and Fletcher, E. A., "Exploratory Investigation of Aerodynamic Effects of External Combustion of Aluminum Borohydride in Airstream Adjacent to Flat Plate in Mach 2.46 Tunnel," NACA RM E57E16, July 1957.

[2]Serafini, J. S., Dorsch, R. G., and Fletcher, E. A., "Exploratory Investigation of Static- and Base-Pressure Increases Resulting from Combustion of Aluminum Borohydride Adjacent to Body of Revolution in Supersonic Wind Tunnel," NACA RM E57E15, Oct. 1957.

[3]Dugger, G. L., Deklau, B., Billig, F. S., and Matthews, S. E., "Summary Report on External Ramjet Program," Johns Hopkins Univ., Applied Physics Lab., TG-419, Laurel, MD, Oct. 1961.

[4]Billig, F. S., "A Review of External Burning Ramjets," Johns Hopkins Univ., Applied Physics Lab., TG-801, Laurel, MD, Dec. 1965.

[5]Dugger, G. L., Billig, F. S., and Avery, W. H., "Recent Work in Hypersonic Propulsion at the Applied Physics Laboratory, the Johns Hopkins University," Johns Hopkins Univ., Applied Physics Lab., TG-355, Laurel, MD, Nov. 1959.

[6]Dugger, G. L., "Comparison of Hypersonic Ramjet Engines with

Subsonic and Supersonic Combustion," *Fourth AGARD Colloquium, Combustion and Propulsion, High Mach Number Airbreathing Engines*, Pergamon, Oxford, England, UK, 1961, pp. 84–119.

[7]Weber, R. J., and MacKay, J. S., "An Analysis of Ramjet Engines Using Supersonic Combustion," NACA TN 4386, Sept. 1958.

[8]Dugger, G. L., Billig, F. S., and Avery, W. H., "Hypersonic Propulsion Studies at APL/JHU," Johns Hopkins Univ., Applied Physics Lab., TG-405, Silver Spring, MD, June 1961.

[9]Keirsey, J. L., "A Study of the Aerodynamics of Scramjet Engine Inlets," Johns Hopkins Univ., Applied Physics Lab., TG-732, Laurel, MD, Sept. 1965.

[10]Dugger, G. L., Avery, W. H., Billig, F. S., Blevins, R. W., Cramer, R. H., George, J. F., Hardgrave, E. J., Hill, M. L., Keirsey, J. L., and Walker, J. H., "A Supersonic Combustion Ramjet Missile (SCRAM) for Naval Missions," Johns Hopkins Univ., Applied Physics Lab., TG-640, Laurel, MD, Jan. 1965.

[11]Waltrup, P. J., Billig, F. S., Funk, J. A., and Dugger, G. L., "Development and Testing of Hypersonic Ramjet Engine," 1974 JANNAF Propulsion Meeting, Oct. 1974; also CPIA Publ. 250, Vol. II, Pt. 1, Feb. 1975, pp. 189–212.

[12]Billig, F. S., Grenleski, S. E., and Pirkle, J. C., "Ignition and Combustion Characteristics of Liquid Fuels for Hypersonic Ramjets," 12th JANNAF Liquid Propulsion Meeting, Vol. 1, CPIA Publ. 201, Oct. 1970.

[13]Orth, R. C., Billig, F. S., Waltrup, P. J., and Cameron, J. M., "Direct-Connect Tests of Supersonic Combustors and Nozzles with Various Fuels at Simulated Mach 7, High Altitude Flight Conditions," 12th JANNAF Combustion Meeting, Vol. III, CPIA Publ. 273, Aug. 1975, pp. 233–253.

[14]Waltrup, P. J., Orth, R. C., Funk, J. A., and Dugger, G. L., "Development and Testing of a Supersonic Combustion Ramjet (SCRAM) Missile," 1976 JANNAF Propulsion Meeting, Vol. IV, CPIA Publ. 280, Dec. 1976, pp. 407–430.

[15]Billig, F. S., Funk, J. A., Waltrup, P. J., and Dugger, G. L., "Design and Testing of Hypersonic Ramjet Engine," 1972 JANNAF Propulsion Meeting, Vol. III, CPIA Publ. 228, Nov. 1972; also April 1973, pp. 293–325.

[16]Billig, F. S., Grenleski, S. E., and Orth, R. C., "Studies of Heat Transfer and Shear in Supersonic Combustors," *AIAA 7th Propulsion Joint Specialist Conference*, CPIA Publ. 213, June 1971, pp. 285–309.

[17]Billig, F. S., and Grenleski, S. E., "Direct Connect and Free Jet Test of SCRAM Engine," *AIAA 5th Propulsion Joint Specialist Conference*, June 1969.

[18]Billig, F. S., and Grenleski, S. E., "Development of a Liquid-Fueled Hypersonic Ramjet Engine," Johns Hopkins Univ., Applied Physics Lab., TG-939, Laurel, MD, Jan. 1969.

[19]Billig, F. S., Waltrup, P. J., and Stockbridge, R. D., "The Integral-Rocket, Dual-Combustion Ramjet: A New Propulsion Concept," *4th International Symposium on Air Breathing Engines*, 1979, pp. 433–444 (AIAA Paper 79-7094); also *Journal of Spacecraft and Rockets*, Vol. 17, No. 5, 1980, pp. 416–424.

[20]Billig, F. S., "Research on Supersonic Combustion," *Journal of Propulsion and Power*, Vol. 9, No. 4, 1993, pp. 499–514.

[21]Billig, F. S., "Design of Supersonic Combustors Based on Pressure-Area Fields," *Proceedings of the 11th Symposium (International) on Combustion*, The Combustion Inst., Pittsburgh, PA, 1967, pp. 755–769.

[22]Billig, F. S., and Dugger, G. L., "The Interaction of Shock Waves and Heat Addition in the Design of Supersonic Combustors," *12th Symposium (International) on Combustion*, The Combustion Inst., Pittsburgh, PA, 1969, pp. 1125–1139.

[23]Waltrup, P. J., Billig, F. S., and Stockbridge, R. D., "A Procedure for Optimizing the Design of Scramjet Engines," AIAA Paper 78-1110, 1978; also *Journal of Spacecraft and Rockets*, Vol. 16, No. 3, 1979, pp. 163–172.

[24]Billig, F. S., "Combustion Processes in Supersonic Flow," *Journal of Propulsion and Power*, Vol. 4, No. 3, 1988.

[25]Agosta, V. D., and Hammer, S. S., "Scramjet Nozzle Analysis," PSI Propulsion Sciences, Rept. 70-1, Melville, NY, Feb. 1970.

[26]Agosta, V. D., Hammer, S., and Migdal, D., "Scramjet Nozzle Analysis," Johns Hopkins Univ., Applied Physics Lab., Propulsion Sciences, Inc., Final Rept., PSI 71-1, Melville, NY, Feb. 1971.

[27]Billig, F. S., Funk, J. A., Lasky, M., and Dugger, G. L., "SCRAM Free Jet Testing, Component Design and Performance," 1971 JANNAF Combined Propulsion Meeting, Vol. III, CPIA Publ. 219, Nov. 1971, pp. 359–383.

[28]Billig, F. S., Corda, S., and Stockbridge, R. D., "Combustor-Inlet Interaction in Scramjet Engines," *APL Technical Review*, Vol. 2, No. 1, 1990, pp. 118–126.

[29]Billig, F. S., Corda, S., and Pandolfini, P. P., "Design Techniques for Dual Mode Ram-Scramjet Combustors," *Proceedings of the AGARD Hypersonic Combined Cycle Propulsion Conference*, 1990, pp. 23-1–23-20 (AGARD CP 479).

[30]Lucero, E. F., "SCRAM Aerodynamic Design," Research and Development Programs Quarterly Rept., Oct.–Dec. 1973, Johns Hopkins Univ., Applied Physics Lab., C-RQR/73-4, Laurel, MD, 1973.